# *np* scattering measurements at 96 MeV

J. Rahm, J. Blomgren, H. Condé, S. Dangtip, K. Elmgren, N. Olsson, T. Rönnqvist,* and R. Zorro†
*Department of Neutron Research, Uppsala University, Box 535, S-75121 Uppsala, Sweden*

O. Jonsson, L. Nilsson, and P.-U. Renberg
*The Svedberg Laboratory, Uppsala University, Box 533, S-75121 Uppsala, Sweden*

A. Ringbom‡ and G. Tibell
*Department of Radiation Sciences, Uppsala University, Box 535, S-75121 Uppsala, Sweden*

S. Y. van der Werf
*Kernfysisch Versneller Instituut, 9747 AA Groningen, The Netherlands*

T. E. O. Ericson
*CERN, CH-1211 Geneva 23, Switzerland*
*and The Svedberg Laboratory, Uppsala University, Box 533, S-75121 Uppsala, Sweden*

B. Loiseau
*Laboratoire de Physique Nucléaire et de Hautes Energies,§ LPTPE, Université P. & M. Curie, 4 Place Jussieu, 75252 Paris Cedex 05, France*

(Received 2 March 1999; revised manuscript received 9 June 2000; published 1 March 2001)

The differential *np* scattering cross section has been measured at 96 MeV in the angular range $\theta_{\text{c.m.}} = 74–180°$ at the neutron beam facility of the The Svedberg Laboratory in Uppsala. A subset of the data, covering 116–180°, has previously been published. The new, extended angular distribution has been normalized to the experimental total *np* cross section. Between 150° and 180°, the angular distribution is steeper than for most previous measurements and nucleon-nucleon potential predictions. At 180°, the difference amounts to about 10%, implying serious consequences because of the fundamental importance of this cross section. A value of the charged $\pi NN$ coupling constant consistent with our earlier result at 162 MeV has been extracted from the data.

DOI: 10.1103/PhysRevC.63.044001 PACS number(s): 13.75.Cs, 13.75.Gx, 21.30.−x

## I. INTRODUCTION

Recently, we have performed an *np* scattering measurement at 162 MeV [1,2], aiming at a higher accuracy than previous experiments. The *np* scattering cross section is not only of importance for investigations of the fundamental properties of the *NN* interaction, but has also a large impact on several applications, such as fast neutron cancer therapy and accelerator-driven transmutation technologies. The reason is that the *np* cross section is used as a primary standard for measurements of other neutron-induced cross sections in the 0–350-MeV region [3], i.e., other cross sections are normalized to that of *np* scattering. In particular the 180° *np* cross section, i.e., the $H(n,p)$ cross section at 0°, is used for normalization purposes. This cross section therefore has to be known to high precision.

We have shown in our previous work that precision data of the *np* cross section in the backward hemisphere are useful for a determination of the charged $\pi NN$ coupling constant. Both the shape of the angular distribution and the absolute normalization of the data are of crucial importance in this context. The $\pi NN$ coupling constant is fundamental for quantitative discussions of many phenomena in nuclear and particle physics, and it is important to have determinations of it with full control of uncertainties. At present, a discussion goes on concerning appropriate methods to determine this quantity [4,5]. The specific issues concerning precision and systematics using backward *np* scattering to extract the coupling constant are addressed in Refs. [2,6,7], providing answers to criticisms discussed in Ref. [8]. The present experiment contributes additional material.

An investigation of the *np* scattering data situation, from 100 to 1000 MeV, up to the present date [9], shows that most of the data seem to fall into two main ''families'' with respect to the angular shape. Two of the largest data sets, i.e., those of Bonner *et al.* [10] (160–800 MeV) and of Hürster *et al.* [11] (200–590 MeV), agree reasonably well in shape above 500 MeV, but differ at 200 MeV by as much as 10–15 % in the 180°/150° cross section ratio. The shape of our previous angular distribution at 162 MeV is in good agreement with that of the Hürster data when plotted as $d\sigma/dt$ ($t$ is the Mandelstam variable), but is, accordingly, in conflict

*Present address: Gammadata AB, Box 15120, S-75015 Uppsala, Sweden.

†Present address: Tandem Accelerator Laboratory, Uppsala University, Box 535, S-75121 Uppsala, Sweden.

‡Present address: National Defense Research Establishment (FOA), S-17290 Stockholm, Sweden.

§Unité de Recherche des Universités Paris 6 et Paris 7, associée au CNRS.

 

with the Bonner data. It is an experimental fact that there is a scaling with energy of the backward differential cross section (see, e.g., p. 376 of Ref. [12]). This is natural, since any potential model with pion exchange gives a $d\sigma/dt$ which varies slowly with energy in the laboratory system to leading order. The observed similarities in shape and normalization at different energies are therefore relevant and they are a clear signature of the charged pion exchange.

Normalization of $np$ scattering differential cross sections has been—and is—a notorious problem [9]. To measure absolute cross sections, either the neutron beam intensity, or some other cross section to which the $np$ scattering can be related, has to be known to high precision. The beam intensity can only be measured using a nuclear reaction, most frequently $np$ scattering. Therefore most experimental data are assigned an absolute precision of no better than 5–10 %, or are just given as relative cross sections.

Below the opening of the pion-production channel at about 270 MeV there is, however, a very direct and precise way of solving the normalization problem in principle. The total $np$ cross section can be determined very accurately (better than 1%) without knowledge of the absolute beam intensity. The total cross section and the differential $np$ cross section are closely linked; if the full angular distribution of the differential cross section is known, an unambiguous normalization to the total cross section can be performed, because all channels but elastic scattering are very small. This technique has been employed in several previous measurements, and is also utilized in the present work. A prerequisite is, however, that a large fraction of the angular distribution is measured.

Recently, the development of a well characterized tagged neutron beam at IUCF [13] opens up another possibility to measure absolute neutron cross sections directly of, e.g., $np$ scattering, to the 1–2 % level. Agreement between precision data taken with these very different techniques would strongly increase the confidence in the absolute scale.

These facts motivate new, precise determinations of the $np$ scattering cross section at several energies, with an angular coverage that is as large as possible. In this paper, we present data from a measurement of the differential $np$ scattering cross section at 96 MeV in the angular range $\theta_{\mathrm{c.m.}} = 74° - 128°$. These data have been linked to the angular distribution measured in 1991 at $\theta_{\mathrm{c.m.}} = 116° - 180°$ by Rönnqvist *et al.* [14]. Both experiments were performed by the same collaboration and with the same experimental setup at the neutron beam facility at the The Svedberg Laboratory (TSL) in Uppsala. Thus the present work is an extension of the Rönnqvist data, now covering the angular range $\theta_{\mathrm{c.m.}} = 74° - 180°$.

Section II of the paper contains a brief description of the experimental arrangement, while the analysis procedure and the important normalization technique are described and discussed in Sec. III. The results are presented and compared with other data, partial-wave analyses (PWA's), and $NN$ potential predictions in Sec. IV. Extrapolation of the data to the pion pole gives a value for the charged $\pi NN$ coupling constant. The analysis and results are presented and discussed in Sec. V. Finally, a summary and the conclusions are given in Sec. VI.

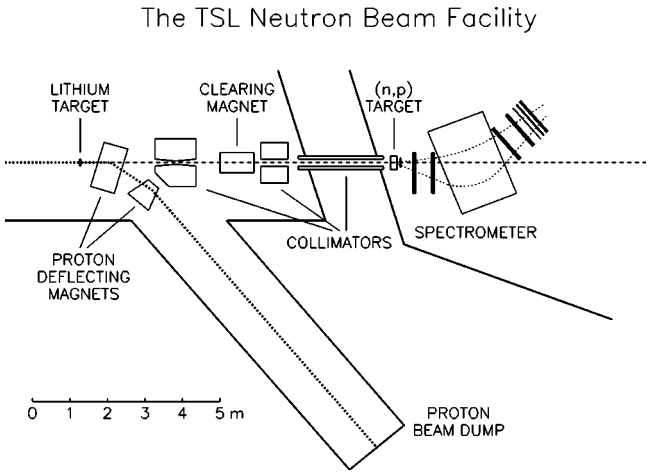


FIG. 1. Overview of the Uppsala neutron beam facility. The neutron production, shielding, and collimation are shown, as well as the magnetic spectrometer arrangement.

## II. EXPERIMENTAL ARRANGEMENT

The experimental setup and procedure have been described in detail recently [2,15], and therefore only a brief summary will be given here.

The TSL neutron beam facility is shown in Fig. 1. Protons from the cyclotron impinge on the neutron production target from the left in the figure. Neutrons are produced by the $^7\mathrm{Li}(p,n)^7\mathrm{Be}$ reaction, using a 214-mg/cm$^2$-thick lithium target, enriched to 99.98% in $^7$Li. After the target, the proton beam is bent into a well-shielded beam dump. The neutron beam is defined by a 1-m-long collimator, with two other collimators serving as beam scrapers. The vacuum system is terminated after the first collimator with a 1-mm-thick aluminum plate. Charged particles produced in this plate are deflected by a clearing dipole magnet. The diameter of the neutron beam at the $np$ target position, 8 m from the neutron production target, is about 7 cm. The neutron yield is in the order of $10^6$ s$^{-1}$ over the full target area. The centroid of the full-energy peak in the neutron spectrum is determined to be $96 \pm 0.5$ MeV. The total energy spread in the peak is estimated to be 0.9 MeV [full width at half maximum (FWHM)].

To maximize the count rate without impairing the energy resolution, a sandwiched multitarget system is used. It consists of thin target layers interspaced by nine multiwire proportional chambers (MWPC's), each having an efficiency of $\geqslant 99\%$. In this way, it is possible to determine in which target the scattering or reaction takes place, so that corrections for energy losses in the subsequent targets can be applied. The first two MWPC's provide veto signals for rejection of the few charged particles that contaminate the neutron beam. The target box contains five 35-mg/cm$^2$-thick $CH_2$ targets and two 85-mg/cm$^2$ $^{12}$C targets, the latter for subtraction of the carbon contribution to the $CH_2$ spectra. The tar-

gets are stacked in the following (downstream) order: 2 $CH_2$, 2 carbon, and 3 $CH_2$ layers.

The momentum determination of the charged particles emitted from the targets is performed with a spectrometer consisting of a dipole magnet and four drift chambers (DCH's) [16], two in front of and two behind the magnet. The scattering angle is determined by the trajectory through the first two DCH's. The detection efficiency for a drift chamber plane is typically $\geqslant 98\%$. To minimize the multiple scattering of charged particles in air, the space between the first two DCH's and the volume in the pole gap is filled with helium gas.

The trigger signal is generated by a coincidence between a small 1-mm-thick plastic scintillator, located immediately after the multitarget box and a large 2-mm-thick plastic scintillator, positioned behind the last DCH. In addition, two large plastic scintillators of thicknesses 4 and 10 mm, respectively, are added behind the 2-mm plastic scintillator, to facilitate particle identification.

The entire setup can be rotated around a pivot point, located below the center of the multitarget box. With one position and one magnetic-field setting, the spectrometer has a horizontal angular acceptance of about 15° in the laboratory system. Measurements are performed with two different settings of the spectrometer position, covering the proton recoil angular ranges $\theta_{LAB}=26°-41°$ and $35°-53°$, respectively. Under these conditions, the energy resolution in the measured spectra is typically in the range 3–5 MeV (FWHM). The angular resolution due to multiple scattering is estimated to be $0.6°-1.3°$ (rms).

## III. DATA ANALYSIS

### A. Data reduction and corrections

The data are analyzed off-line on an event-by-event basis. Before an event is accepted, a number of tests are applied. A brief summary of the analysis procedure is given below. More detailed information about the data reduction has been given in Ref. [2].

Events originating from charged particles contaminating the neutron beam, or from charged-particle production in the thin scintillator just after the target system, are rejected. The scattering angle is determined by calculating the particle trajectory through the first two DCH's, using both the horizontal and vertical coordinate information. The particle momentum is determined by a ray-tracing procedure, using magnetic field maps and position information from the DCH's. Three DCH's are required for this purpose. The use of the fourth DCH offers a possibility for a redundancy check. The few events with dubious energy determination, or with a trajectory outside the magnetic-field limits or an origin outside the neutron beam spot are rejected. To avoid vertical acceptance corrections, a narrow software gate of $\pm 0.8°$ is applied on the vertical scattering angle, ensuring that no events are lost in the magnetic gap. The momentum information, in combination with the pulse heights from two of the large scintillators, is used to discriminate between protons and other charged particles (almost exclusively deuterons).

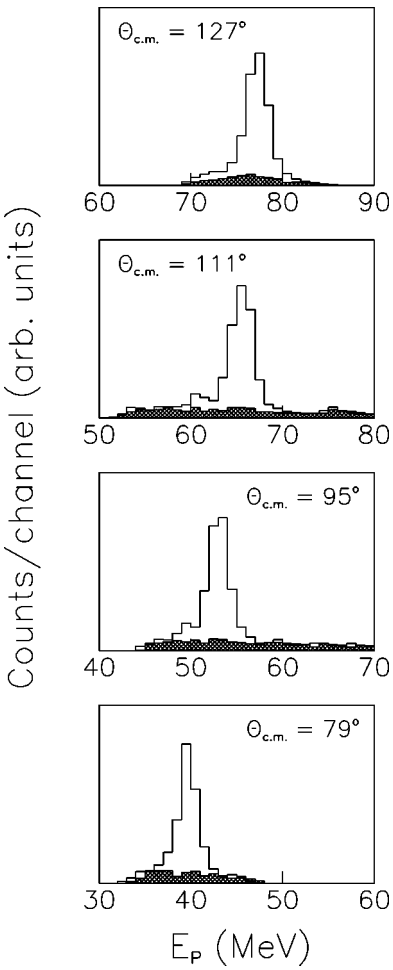


FIG. 2. Proton energy spectra from $CH_2$ (open histograms) and carbon (cross-hatched histograms) targets, respectively, at various scattering angles. The part of the $CH_2$ spectra at lower energies not accounted for by the carbon contribution originates from *np* scattering of neutrons from the low-energy neutron tail.

All accepted events are stored in matrices with angular and energy binning in the laboratory system of 1° and 0.25 MeV, respectively. Before extracting the hydrogen peak content, the carbon contribution to the $CH_2$ spectra is subtracted. This is illustrated for a few angles in Fig. 2, where an energy binning of 1 MeV is used. The open histograms represent the energy spectra from the $CH_2$ foils, while the cross-hatched histograms are those of the pure carbon targets, after normalization to the same number of target nuclei.

The *np* scattering peak contents are determined by integration. Since the energy resolution varies with angle, different integration windows are used. These are defined in a consistent way, and the final peak contents are determined by integrating the data in a region of $\pm\Delta E$ around the centroid, where $\Delta E$ is the peak FWHM. With this definition, the carbon background amounts to maximum 15% of the hydrogen peak for the largest recoil angles.

The variation of the width of the *np* peak with angle also causes an angular dependence in the background contribution from the low-energy continuum of the $^7$Li$(p,n)$ reaction. The data are corrected for this effect by using experi-

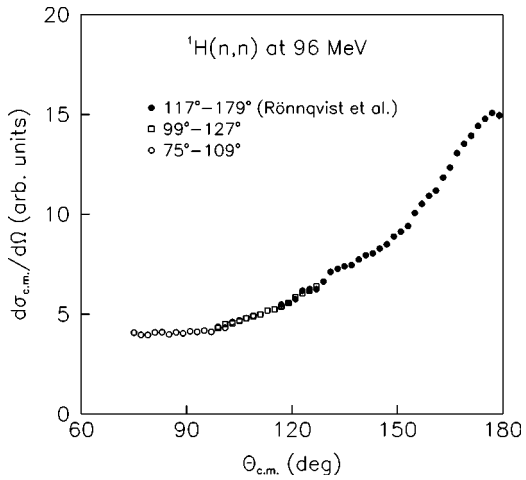


FIG. 3. Relative differential $np$ scattering cross sections at $E_n = 96$ MeV. The open symbols represent data from the two magnetic settings, while the filled circles are the previously published backward-angle data [14]. The three data sets were normalized to each other in the overlapping regions.

mental neutron spectra from this reaction determined by Byrd and Sailor [17] at $E_p = 90.1$ and 139.9 MeV. To simulate the finite resolution of our experiment, the Byrd and Sailor spectra, which have a much better resolution than in the present experiment, are folded with Gaussian resolution functions. From these folded spectra, the neutron continuum contribution to the peak, as defined above, can be determined as a function of peak width, and appropriate relative correction factors ($<3\%$) can be determined.

Since the energy of the recoil protons varies with scattering angle, the variation of the proton absorption with energy in the detector system has to be taken into account. To first order, elastic in- and out-scattering of protons cancel, and thus only nonelastic losses have to be considered. We have calculated these losses in the targets, detectors, and helium gas, using the total reaction cross sections given by Carlson [18]. The proton attenuation gives non-negligible corrections only in the angular region $\theta_{\mathrm{c.m.}} = 74° - 110°$, and the maximum correction amounts to 1.8% (at 74°).

### B. Relative cross sections and uncertainties

The relative cross section data from the two different spectrometer settings, together covering the 74°–128° (c.m.) angular region, are used to extend the data of Rönnqvist *et al.* [14]. The three individual data sets, all treated as relative cross sections, are matched pairwise in the two uncorrelated overlapping regions using a minimum $\chi^2$ criterion [2]. The result of this matching is shown in the c.m. system in Fig. 3. As can be seen, the agreement in shape in the overlapping regions is very good. Final relative $np$ scattering cross sections are obtained by averaging the data from the different data sets in each 2° (c.m.) angular bin. A similar matching procedure was used by Rönnqvist *et al.* for five data sets to generate the full angular distribution. It should be pointed out that the five Rönnqvist sets, which were taken at different occasions, essentially fall into two main angular regions, i.e., 148°–180° and 116° to about 156°, respectively. Thus there is a significant overlap of these two regions. Furthermore, there is no systematic shape difference between distributions with similar angular coverage, which is also verified by the small $\chi^2$'s mentioned.

Many sources of uncertainties contribute to the total error in the relative cross section. These errors are of both random and systematic character. Since the measurement is relative, only those systematic errors that affect the shape of the angular distribution have to be considered.

The random error is dominated by counting statistics, giving a contribution in the range 1.0–2.7 % per point for the new data. The smaller value is valid for the data points close to 127°. Another small, random error contribution is due to bin truncation when integrating the $np$ peak. This error is at most 0.6% per point.

The most important contribution to the systematic error is related to the subtraction of the carbon background in the $CH_2$ energy spectra. Above about 145° the hydrogen peak is well separated from the carbon spectrum ($Q$ value $= -12.6$ MeV), and below 125° the hydrogen peak is superimposed on a flat carbon continuum. In the latter region the uncertainty in the relative thickness of the $CH_2$ and pure carbon targets introduces an error in the $np$ cross section. With an estimated relative thickness uncertainty of 5%, the error in the angular region 75°–127° is less than 0.7%.

In the angular range 125°–145° the hydrogen peak interferes with the rising slope of the carbon background. Hence a small error in the relative energy loss corrections for the $CH_2$ and carbon spectra, respectively, affects the background subtraction. This causes an error in the determined $np$ cross section of $<2\%$, using an estimated relative energy uncertainty of $\pm 1$ MeV. The problems arising from this effect can be seen in the Rönnqvist *et al.* [14] data around 133° in Fig. 3. Since the effect occurs in the middle of one of the Rönnqvist angular settings, it is not expected to contribute significantly to a possible progressive shape uncertainty arising from the overlap normalization procedure.

The correction ($<3\%$) for the contribution from the low-energy continuum of the $^7$Li$(p,n)$ spectrum to the $np$ scattering peak introduces a systematic error that varies with the peak width and thus with the angle. Assuming a relative uncertainty of 10% in the correction, an error in the data of at most 0.3% arises.

The error from the small correction due to the energy-dependent attenuation of the protons is estimated to be less than 0.6%.

When adding the various systematic uncertainties quadratically, the total systematic error varies from 0.5 to 2.0 % in the full angular region. The largest errors are found in the range $\theta_{\mathrm{c.m.}} = 125° - 145°$.

In addition to the random and systematic errors discussed, the shape of the full angular distribution is affected by the matching of the data sets. A quadratic addition of the uncertainties in the fitted coefficients, emerging mainly from the finite counting statistics, results in a shape error of $\pm 2.1\%$ between the most forward and most backward data sets, i.e., in the 75°/179° cross section ratio. This slope error includes the corresponding uncertainty of $\pm 1.3\%$ from the Rönnqvist *et al.* data. There could in principle be additional slope errors

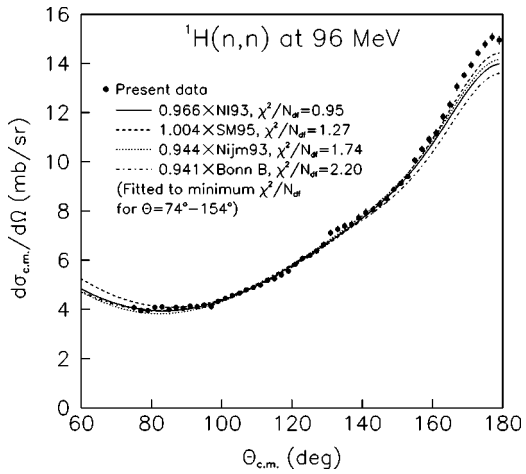


FIG. 4. Relative differential *np* scattering cross sections at $E_n = 96$ MeV. The filled circles represent the present data, while the solid and dashed lines are the SM95 [20] and NI93 [27] PWA's, respectively, and the dotted and dot-dashed lines are the Nijm93 [27] and Bonn B [26] *NN* potentials, respectively, all least-squares fitted to the data in the angular region 74°–154°.

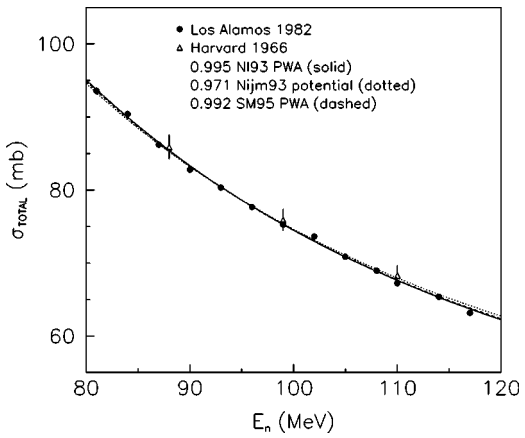


FIG. 5. Total *np* cross section versus energy in the range 80–120 MeV. The different symbols represent experimental data [21,22], while the lines are from PWA's and *NN* potentials, renormalized by us to the data in the shown energy region.

caused by small inhomogeneities in the drift chamber efficiencies, which could amplify from one setting to the next one. This does not seem probable, however, since 75% of the angular distribution, i.e., from 74° to 154°, is extremely well described by the PWA's. This is shown in Fig. 4, where the normalization of the NI93 [19] and SM95 [20] PWA's have been least-squares fitted to the experimental data in the angular range 74°–154°. The $\chi^2$ per degree of freedom is 0.95 and 1.27 with respect to the NI93 and SM95 PWA's, respectively. Lowering the upper angle limit point by point results in fits with similar quality, while increasing it leads to a rapidly increasing $\chi^2$ per degree of freedom. Thus shape deviations from these models are found only beyond 154°, which is within one of the angular settings, and more or less outside the overlap region for the next setting. For comparison we show also in this figure similar least-square fits for the Nijmegen (Nijm93) and Bonn B potentials with $\chi^2$ per degree of freedom of 1.74 and 2.20, respectively. One can see that in the 74°–154° region the shape of the Nijm93 potential angular distribution is closer to that of the data than the shape of the Bonn B potential.

### C. Normalization procedure

Absolute *np* scattering cross sections are obtained by normalization to the total *np* cross section, which can be done since other reaction channels are negligible at 96 MeV. The total cross section $\sigma_T$ has been experimentally determined around 100 MeV by several groups, and is considered to be well known. If the entire angular range, i.e., from 0° to 180°, had been measured in the present experiment, it would have been possible to normalize the data to the total cross section directly by integration. Since that is not the case, we consider our angular distribution as a measurement of a *fraction* of the total cross section, i.e., the part between 74° and 180°. By using a number of PWA's or potential models, it is possible to estimate the magnitude $F$ of this fraction, to which the data should be normalized. Thus we require that the integral over the solid angle of our data should be equal to

$$\sigma_{74^\circ-180^\circ} = \int_{74^\circ}^{180^\circ} \frac{d\sigma}{d\Omega} d\Omega = F \sigma_T^{exp}, \tag{1}$$

where

$$F = \sigma_{74^\circ-180^\circ}^{PWA} / \sigma_T^{PWA}. \tag{2}$$

To obtain $\sigma_T^{exp}$, we have used the Los Alamos data of Lisowski *et al.* [21], and the Harvard data of Measday and Palmieri [22]. The total error of the former is below 1% and of the latter about 4%. These data are in very good agreement. At slightly higher energies, i.e., above 125 MeV, one has also excellent agreement between these data and those from PSI by Grundies *et al.* [23], for which the errors are less than 1.5%.

The total cross section at 96 MeV is determined by fitting the absolute scale of the Nijmegen energy-dependent PWA NI93 [19] to the experimental data in the energy region 80–120 MeV, as illustrated in Fig. 5. A slight renormalization of 0.995 is needed to obtain a good fit. Also other PWA's and potentials have been tested, but it is found that NI93 gives the best description of the energy dependence of $\sigma_T^{exp}$. The resulting total cross section at 96 MeV is

$$\sigma_T^{exp} = 77.74 \pm 0.78 \pm 0.43 = 77.74 \pm 0.89 \text{ mb}, \tag{3}$$

where the first error corresponds to the 1% systematic error of the Lisowski data, and the second error is due to the $\pm 0.5$ MeV uncertainty in the neutron beam energy, because the total cross section has a slope of 1.11%/MeV.

The fraction $F$ of the total cross section covered in the present experiment is determined from the PWA's SM95 [20], VL40 [3], and VZ40 [24] of VPI, and NI93 of Nijmegen [19]. VL40, VZ40, and NI93 are energy-dependent PWA's based on data in the 0–350 or 400 MeV region, while SM95 was obtained by fitting up to 1.6 GeV. The result is given in Table I, together with integrated cross

TABLE I. Total cross sections ($\sigma_T$) and angular fractions ($F = \sigma_{74°-180°}/\sigma_T$) for different PWA's and *NN* potential models. The weighted experimental value is 77.74 mb (see the text for more details).

| PWA or potential | $\sigma_T$ | $\sigma_{0°-74°}$ | $\sigma_{74°-180°}$ | $F$ | $\sigma_T^{exp}/\sigma_T$ |
|---|---|---|---|---|---|
| SM95 [20] | 78.22 | 30.88 | 47.34 | 0.6052 | 0.9939 |
| VZ40 [24] | 77.52 | 30.22 | 47.30 | 0.6102 | 1.0028 |
| VL40 [3] | 77.70 | 30.19 | 47.51 | 0.6115 | 1.0005 |
| NI93 [19] | 78.07 | 29.30 | 48.77 | 0.6247 | 0.9958 |
| Average | 77.88 | 30.15 | 47.73 | 0.6129 | 0.9982 |
| Paris [25] | 79.75 | 29.80 | 49.95 | 0.6263 | 0.9748 |
| Bonn B [26] | 77.96 | 28.95 | 49.01 | 0.6287 | 0.9972 |
| Nijm93 [27] | 79.99 | 30.12 | 49.87 | 0.6235 | 0.9719 |

sections and fractions for the Paris [25], Bonn B [26], and Nijmegen [27] (Nijm93) potentials for comparison. For the final value of $F$ we take the average of the four mentioned PWA's to obtain $F=0.613$. The potential models are not included in the determination, because we believe that the PWA's are more reliable since they describe the total cross section better. Thus the integrated *np* scattering data have been normalized to

$$\sigma_{74°-180°}^{exp} = F\sigma_T^{exp} = 0.613 \times 77.74 = 47.65 \text{ mb}. \quad (4)$$

The result is shown in Fig. 6(a), where the differential cross section has been multiplied with the solid angle element $2\pi \sin\theta$. In this representation, each angle bin directly shows its contribution to the total cross section. Also shown in the figure are the PWA's used to determine $F$, after normalization to $\sigma_T^{exp}=77.74$ mb. As was discussed in the previous section, the data are well represented by any of the PWA's in most of the covered angular region. Deviations occur only at the extreme backward angles which, however, carry only small contributions to the total cross section [see Fig. 6(a)].

The spread in $F$ for the various PWA's and *NN* potential models can be used to estimate the precision of this normalization procedure. One can see from Table I that the maximum deviation from the average value is $-1.3\%$ for the SM95 solution and $+2.6\%$ for the Bonn B potential. From this comparison, we believe that it is fair to say that the normalization uncertainty is within $\pm 1.5\%$. In addition, we have the ''intrinsic'' uncertainty in $\sigma_T^{exp}$ of 1.1%. Summing these effects yields a total normalization uncertainty of $\pm 1.9\%$. However, a word of caution should be given here: The estimated uncertainty relies on the assumption that the various models give a reasonable account of the main characteristics of the angular distribution. If the balance between the two humps at about 40° and 130° seen in Fig. 6(a) is considerably different, our normalization would of course be affected. If, e.g., the cross section in the forward hemisphere is larger than predicted by the models, this has to be compensated by lower backward cross sections to conserve the total cross section, and in this case our normalization would have to be lower.

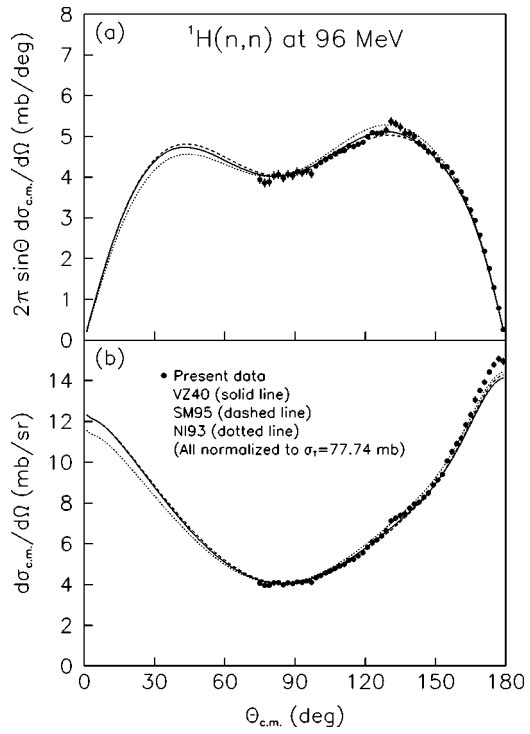


FIG. 6. Angular distributions for the SM95 [20], VZ40 [24], and NI93 [27] PWA's, and the present experimental data (filled circles) at 96 MeV. The VL40 [3] PWA solution is almost identical to VZ40 and is not shown for clarity. (a) Differential *np* scattering cross sections multiplied by the solid angle element $2\pi \sin\theta$. (b) Differential cross sections for *np* scattering.

## IV. EXPERIMENTAL RESULTS

The final experimental differential cross sections are given in Table II and are shown as filled circles in Fig. 6(b). The errors given are the quadratic sums of the statistical and systematic uncertainties of the relative cross sections discussed above. They do not include, however, the normalization uncertainty of $\pm 1.9\%$ and the shape uncertainty of $\pm 2.1\%$ between the most forward and backward data sets, i.e., in the 75°/179° cross section ratio. These errors are correlated, and thus no individual point has a normalization error larger than about 2.2%. Also shown in the figure are the PWA's used to determine the normalization. As can be seen, the data are steeper than the PWA's in the 154°–180° region, while they are well described at smaller angles, as has been discussed earlier. As can be expected from the figure, and as has been mentioned in Ref. [8], these data and those of our previous measurement at 162 MeV [2] lead to a very high $\chi^2$ for the PWA NI93 [19].

The present extension in angular range of the previous Rönnqvist *et al.* data [14] leads to a 1% higher normalization for the latter, which is well within the 4% normalization error stated in that work.

The new 96 MeV data are compared with other experi-

TABLE II. Differential cross sections for *np* scattering at 96 MeV.

| $\theta_{\text{c.m.}}$ (deg.) | $d\sigma/d\Omega$ (mb/sr) | $\theta_{\text{c.m.}}$ (deg.) | $d\sigma/d\Omega$ (mb/sr) | $\theta_{\text{c.m.}}$ (deg.) | $d\sigma/d\Omega$ (mb/sr) |
|---|---|---|---|---|---|
| 75.0 | 4.075±0.109 | 111.0 | 4.985±0.068 | 147.0 | 8.492±0.151 |
| 77.0 | 3.957±0.108 | 113.0 | 5.181±0.068 | 149.0 | 8.886±0.101 |
| 79.0 | 3.956±0.106 | 115.0 | 5.240±0.069 | 151.0 | 9.128±0.101 |
| 81.0 | 4.080±0.106 | 117.0 | 5.393±0.063 | 153.0 | 9.401±0.101 |
| 83.0 | 4.098±0.105 | 119.0 | 5.556±0.064 | 155.0 | 10.067±0.121 |
| 85.0 | 3.988±0.103 | 121.0 | 5.836±0.066 | 157.0 | 10.522±0.121 |
| 87.0 | 4.083±0.103 | 123.0 | 6.073±0.068 | 159.0 | 10.915±0.141 |
| 89.0 | 4.038±0.102 | 125.0 | 6.190±0.069 | 161.0 | 11.178±0.141 |
| 91.0 | 4.132±0.102 | 127.0 | 6.371±0.069 | 163.0 | 11.834±0.141 |
| 93.0 | 4.111±0.101 | 129.0 | 6.634±0.121 | 165.0 | 12.329±0.151 |
| 95.0 | 4.170±0.100 | 131.0 | 7.119±0.131 | 167.0 | 13.056±0.162 |
| 97.0 | 4.110±0.098 | 133.0 | 7.260±0.131 | 169.0 | 13.520±0.121 |
| 99.0 | 4.328±0.055 | 135.0 | 7.391±0.141 | 171.0 | 13.934±0.131 |
| 101.0 | 4.442±0.056 | 137.0 | 7.452±0.141 | 173.0 | 14.429±0.131 |
| 103.0 | 4.560±0.056 | 139.0 | 7.735±0.141 | 175.0 | 14.783±0.141 |
| 105.0 | 4.660±0.056 | 141.0 | 7.947±0.141 | 177.0 | 15.075±0.151 |
| 107.0 | 4.789±0.057 | 143.0 | 8.038±0.141 | 179.0 | 14.944±0.172 |
| 109.0 | 4.898±0.057 | 145.0 | 8.280±0.141 | | |

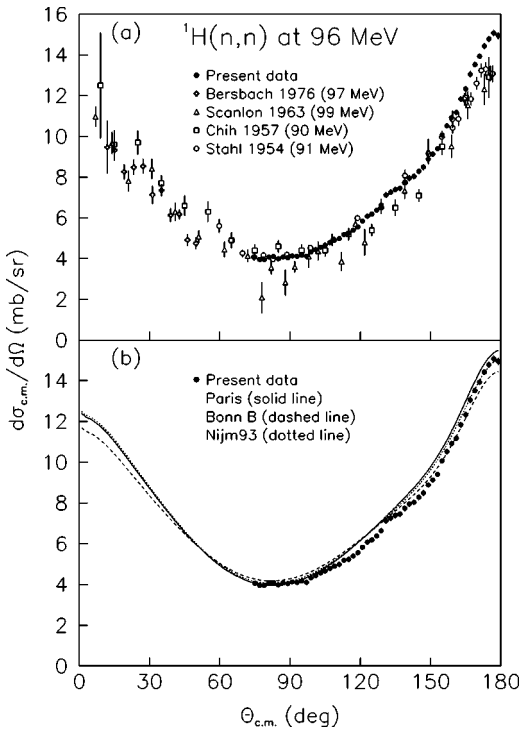


FIG. 7. (a) Differential *np* scattering cross sections of the present work (filled circles). Also plotted are other data from the literature at energies close to 96 MeV [28–31]. (b) The present differential cross sections plotted together with the Paris [25], Bonn B [26], and Nijm93 [27] *NN* potentials.

mental data from measurements performed close to that energy in Fig. 7(a). Thus we give in the figure the data of Stahl and Ramsey [28], Chih and Powell [29], Scanlon *et al.* [30], and Bersbach *et al.* [31]. It can be seen in the figure that the present data are higher at the most backward angles, which indicates a larger steepness at those angles. The PWA's and the potential models have been adjusted to the Bonner data at higher energies, as well as to these earlier, not very precise, data. A comparison to the various models is therefore more instructive than a direct comparison to the data. From the study made in the last paragraph of Sec. III B, the result of which was shown in Fig. 4, one can conclude that the shape of our backward differential cross section, i.e., for angles beyond 154°, is clearly steeper than that of the models, and thus also steeper than the older data. Our data has also a larger 180°/90° cross section ratio.

The Stahl and Ramsey data [28] at 91 MeV from Harvard are included in the fits of the VPI PWA's, but not in that of the Nijmegen group. The experiment covered scattering angles between 60° and 180°, comprising in total 25 data points. The data were normalized to the total cross section, at that time believed to be 78.5±3 mb (the present value is 82.0 mb [21]). For the region not covered by the experiment, other *np* experimental data were used. The normalization error was assumed to be ±5%.

The Chih and Powell [29] data at 90 MeV consist of 18 points distributed over the angular range 8°–180°. The measurement, which was performed with a cloud chamber, was relative and was normalized to a total *np* cross section of 76.0 mb (the present value is 82.8 mb). The normalization uncertainty is not discussed in the paper. The data are included in the Nijmegen PWA fit, but are not present in the VPI data base.

The Scanlon *et al.* data [30] at 99 MeV from Harwell cover the angular range from 7° to 173° in the c.m. system. Absolute cross sections between 7° and 120° were deduced by measuring the count-rate ratio between scattered neutrons and those of the direct neutron beam. Between 80° and 173°, the recoil protons were detected and only relative values for the cross sections could be obtained. This data set was normalized to the small-angle set in the 80°–120° region. Absolute values were also determined by normalizing to the *np* total cross section. The final differential cross sections, shown in Fig. 7(a), were obtained by combining the results of the two methods. The normalization uncertainty was claimed to be better than ±4%. The Scanlon data have been under critical examination by Hammans *et al.* [32] and Henneck [33], who recommend rejection of these data, based on experimental problems. The Nijmegen group has removed these data from their PWA fit, while the VPI group includes them in all their PWA versions.

The 97-MeV data of Bersbach *et al.* [31] were measured between 10° and 50° in the c.m. system, and are included in both the Nijmegen and VPI PWA fits. The normalization uncertainty was estimated to be ±10%. Like the Scanlon forward-angle data, absolute cross sections were obtained from scattered versus direct beam count-rate ratios.

The older data show a larger spread than the present ones, and it is therefore difficult to judge upon the degree of agreement. Furthermore, they are taken at slightly different energies, which affect the shape of the angular distribution. If the Stahl and Ramsey data, which show the smallest spread of

the old data sets, are corrected for the energy difference (91 vs 96 MeV) using the NI93 PWA, which increases the 180°/90° cross section ratio by about 7%, they agree fairly well with the present ones up to 175°, after upward renormalization of about 10%.

In Fig. 7(b), the present data are compared with three $NN$ potential models, namely the Paris [25], Bonn B [26], and Nijm93 [27] potentials. The angular distributions of the Paris and Nijm93 potentials are rather similar, and describe the data reasonably well in the 160°–180° region, while a 7% overprediction is seen in the 110°–160° region. One should keep in mind, however, that both the Paris and Nijm93 potentials overpredict the total cross section by 3%. It is interesting to note that although the Nijm93 potential and the present data do not agree over the entire interval studied, the 180°/90° cross section ratio is in good agreement. The Bonn B potential is relatively close to the data in the 130°–165° region, but underpredicts it at 180° by 6%. This potential gives, on the other hand, a total $np$ cross section which is in good agreement with the experimental one.

## V. DETERMINATION OF THE $\pi NN$ COUPLING CONSTANT

We have in the previous sections achieved our primary aim, which is to give normalized $np$ cross sections. We now briefly explore the bearing these data have on the discussion of the $\pi NN$ coupling constant. We closely follow the procedure previously discussed in our work at 162 MeV to which we refer for details [2]; here we only sketch the procedure. The analysis is based on the fact that the charged pion exchange contributes importantly to the $np$ charge exchange at small momentum transfers. This was realized already in 1958 by Chew, who suggested a model-independent extrapolation to the pion pole for the determination of the coupling constant.

The Chew extrapolation procedure [34,35] is based on a polynomial expansion in the square of the momentum transfer, $q^2$. The technique used to extrapolate to the pion pole is to first construct a smooth physical function, the Chew function, by multiplying the cross section by $(q^2+m_\pi^2)^2$, which removes the pole term, after which the extrapolation can be made far more safely and controlled. Here $m_\pi$ is the charged pion mass. More exactly, in the physical region the function $y(x)$ is defined by

$$y(x)=\frac{sx^2}{m_\pi^4 g_R^4}\frac{d\sigma}{d\Omega}(x)=\sum_{i=0}^{n-1} a_i x^i. \tag{5}$$

Here $s$ is the square of the total energy and $x=q^2+m_\pi^2$. At the pion pole $x=0$, the Chew function gives

$$y(0)\equiv a_0\equiv g_{\pi^\pm}^4/g_R^4 \tag{6}$$

in terms of the pseudoscalar coupling constant $g_{\pi^\pm}^2\simeq 14$. The quantity $g_R^2$ is a reference scale for the coupling chosen for convenience. It is important to realize that the model-independent extrapolation requires accurate data with absolute normalization of the differential cross section. If the differential cross section is incorrectly normalized by a factor $N$, the extrapolation gives $\sqrt{N}g_{\pi^\pm}^2$. This is one of the most important sources of uncertainty in the practical extrapolation from data.

An improvement on this rather slowly converging expansion is the difference method introduced in our previous work at 162 MeV [1,2], and also applied to $\bar{p}p$ charge exchange [36]. The difference method applies the Chew method to the difference between the function $y(x)$ obtained from a model with exactly known coupling constant and from the experimental data, i.e.,

$$y_M(x)-y_{exp}(x)=\sum_{i=0}^{n-1} d_i x^i \tag{7}$$

with $g_R$ of Eqs. (5) and (6) replaced by the model value $g_M$. At the pole

$$y_M(0)-y_{exp}(0)\equiv d_0\equiv\frac{g_M^4-g_{\pi^\pm}^4}{g_M^4}. \tag{8}$$

This procedure should diminish systematic extrapolation errors and remove a substantial part of the irrelevant information at large momentum transfers, provided that the data and the model have a similar behavior at large momentum transfers. Otherwise, the difference method has little advantage as compared with the Chew approach.

As previously, we apply the difference method using four comparison models, i.e., the Nijm93 [27] and Bonn B [26] potentials, the Nijmegen energy-dependent PWA NI93 [19], and the VPI energy-dependent PWA SM95 [20]. The previous $\chi^2$ study performed in the angular range 74°–154° has shown that the NI93 model agrees quite well with the data at large momentum transfers as does the Nijm93 one (cf. Fig. 4). For the region 74°–86° the SM95 model deviates markedly from the data and these are also not very well described by the Bonn B model. Already at this stage one should expect the difference method to work better for the NI93 and Nijm93 models than for the SM95 and Bonn B ones. For the case of the Bonn B potential, some minor modifications must be made in Eq. (8) to account for the fact that it uses an average pion mass of $\bar{m}_\pi=138.03$ MeV, which shifts the pole position. This changes slightly the difference between the model and experimental Chew functions, and induces a small correction[1] for the relation between $g_{\pi^\pm}^2$ and $d_0$. The resulting $y_M(x)-y_{exp}(x)$ are shown in Figs. 8 and 9, together with polynomial fits in $x$ of different orders $n-1$. As can be seen, the error bars blow up at large $x$, which is a

[1]In Eq. (8) one replaces $y_M(x)$ by $\bar{y}_M(\bar{x})=(s\bar{x}^2/m_\pi^4 g_M^4)\ d\sigma/d\Omega_M(\bar{x})$ where $\bar{x}=x+\delta m^2$ with $\delta m^2=\bar{m}_\pi^2-m_\pi^2$. At the pion pole and to first order in $\delta m^2$, $d_0=(\bar{m}_\pi/m_\pi)^4\ [1+\delta m^2 y'_M(0)]-g_{\pi^\pm}^4/g_M^4$ with $y'_M(0)=dy_M(\bar{x})/d\bar{x}|_{\bar{x}=0}$. This gives to first order in $d_0$, $g_{\pi^\pm}^2=g_M^2[1-d_0/2+\delta m^2 y'_M(0)/2]$. Here, $\delta m^2 y'_M(0)/2\simeq 0.01$.

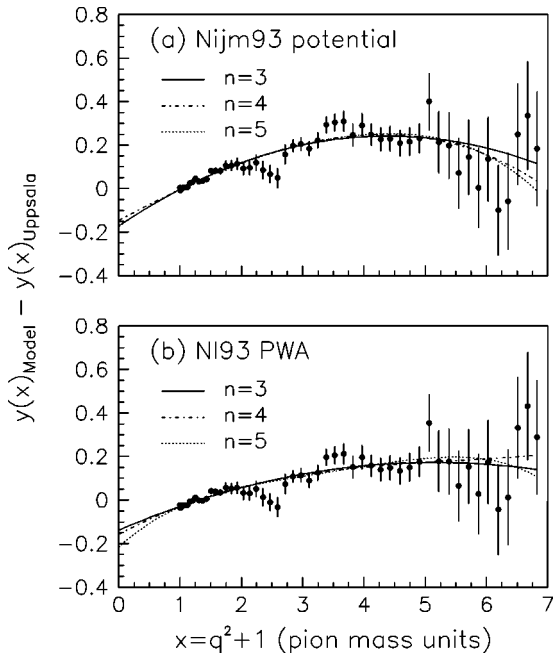


FIG. 8. Extrapolations of the Chew function $y(x)$ to the pion pole at 96 MeV with the difference method using different comparison functions and different polynomials orders. The comparison functions are (a) the Nijm93 potential model [27], (b) the Nijmegen energy-dependent PWA NI93 [19].

consequence of the multiplication of the cross section with $x^2$, leading to a smaller weight for the large $q^2$ region in the extrapolation. Already a visual extrapolation to $x=0$ gives $g^2_{\pi^\pm}$ to a precision of about 3% for any given comparison function in Figs. 8 and 9, especially if one ignores the few

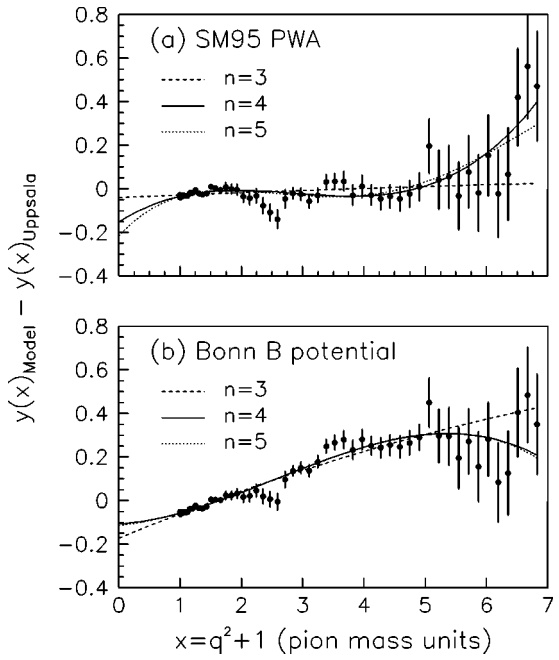


FIG. 9. Same as Fig. 8. The comparison functions are (a) the Virginia energy-dependent PWA SM95 [20], and (b) the Bonn B potential model [26].

points around $x=2.5$, which might be affected by the carbon background subtraction problem around 133° discussed in Sec. III B. For the Nijm93 potential [Fig. 8(a)], the NI93 PWA [Fig. 8(b)], and the SM95 PWA [Fig. 9(a)], $d_0 \simeq -0.15(5)$, leading to $g^2_{\pi^\pm} \simeq 14.60(34)$, 14.60(34), and 14.78(34), respectively. For the Bonn B potential [Fig. 9(b)], $d_0 \simeq -0.14(5)$, which gives $g^2_{\pi^\pm} \simeq 15.26(36)$. This is in agreement with the more sophisticated and accurate analysis below.

The values of the charged coupling constant obtained from the extrapolation using the polynomial fits are given in Table III for the four different comparison models considered here. Let us recall that $n$ is the number of terms in the polynomial expansion, $\chi^2/N_{df}$ is the average $\chi^2$ per degree of freedom and $g^2_{\pi^\pm}$ is the resulting value of the coupling constant, with its statistical and extrapolation error.[2] The behavior of $\chi^2/N_{df}$ as a function of $n$ is characteristic. It falls with increasing $n$ to a nearly constant value with variation less than 2%, corresponding to the usual criterion that a decrease in the total $\chi^2$ by one unit when $n$ is increased by one step, is an indication that the data are overparametrized. In the present case of 53 data points, this occurs when $\chi^2/N_{df}$ changes by less than 2%. Additional terms give only small gains, the data become rapidly overparameterized and the uncertainty large. The values of $g^2_{\pi^\pm}$ remain, however, compatible within errors. We determine $g^2_{\pi^\pm}$ from the first value of $n$ for which $\chi^2/N_{df}$ becomes nearly constant. This is in accordance with standard statistical procedures. The value for $\chi^2/N_{df}$ of 0.93 to 0.95 in Table III is well within the statistically expected range. Note, however, that $\chi^2/N_{df}$ as expected becomes close to unity *on the average* for a large number of pseudoexperiments, when the number of parameters used is sufficient to describe the data well (see Table IV below).

With the Nijm93 potential and NI93 PWA our best choice of $n$ is 3 according to the procedure described in the previous paragraph. This gives a small statistical extrapolation error. Going to $n=4$ gives approximately the same quality of fits and does not really change the extrapolated value of $g^2_{\pi^\pm}$, but the errors become larger. With the SM95 PWA of VPI and the Bonn B potential, the best choice of $n$ is 4. The corresponding $g^2_{\pi^\pm}$ values are larger than those with the previous two models, and so are their uncertainties. While the $g^2_{\pi^\pm}$ using SM95 is compatible within errors to the Nijm93 and NI93 ones, that using Bonn B is slightly larger. The shape of the angular distribution of the Bonn B potential fits the data less well than those of the other models [see Figs. 4, 6(b), and 7(b)]. This difference is most probably responsible for the relatively large $g^2_{\pi^\pm}$ value obtained in this case.

As in our preceding work, we establish the systematic uncertainties of the extrapolation procedure from pseudodata with uncertainties corresponding to those of the present ex-

[2]Recall that this error has only a meaning when the $\chi^2/N_{df}$ is close to 1.

TABLE III. Values of the coupling constant obtained from polynomial fits with $n$terms to data at 96 MeV using the difference method for the full range of data ($0<q^2<5.8\ m_\pi^2$). The experimental values at the minimum $\chi^2/N_{df}$ are indicated in boldface. The comparison models are the Nijm93 [27] and Bonn B [26] potentials, and the NI93 [19] and SM95 [20] energy-dependent PWA's. The model coupling constants are $g^2_{\pi^\pm}$,(Nijm93)$=g^2_{\pi^\pm}$,(NI93)$=13.58$, $g^2_{\pi^\pm}$,(SM95)$=13.75$, and $g^2_{\pi^\pm}$,(Bonn B)$=14.40$.

| $n$ | $\chi^2/N_{df}$ | $g^2_{\pi^\pm}$ | $\chi^2/N_{df}$ | $g^2_{\pi^\pm}$ | $\chi^2/N_{df}$ | $g^2_{\pi^\pm}$ | $\chi^2/N_{df}$ | $g^2_{\pi^\pm}$ |
|---|---|---|---|---|---|---|---|---|
| | Nijm93 − Uppsala | | NI93 − Uppsala | | SM95 − Uppsala | | Bonn B − Uppsala | |
| 2 | 1.917 | 14.11 ± 0.04 | 1.242 | 14.16 ± 0.04 | 1.333 | 14.02 ± 0.04 | 1.107 | 15.34 ± 0.03 |
| 3 | 0.956 | **14.69 ± 0.09** | 0.966 | **14.49 ± 0.09** | 1.359 | 14.03 ± 0.09 | 1.081 | 15.46 ± 0.08 |
| 4 | 0.956 | 14.54 ± 0.18 | 0.974 | 14.61 ± 0.18 | 0.962 | **14.77 ± 0.18** | 0.932 | **15.01 ± 0.18** |
| 5 | 0.971 | 14.71 ± 0.39 | 0.970 | 14.98 ± 0.39 | 0.955 | 15.17 ± 0.38 | 0.951 | 15.07 ± 0.38 |

periment, according to the following procedure. For each of the four models mentioned above, which all have a known coupling constant, we simulate our experimental data by generating 10 000 pseudoexperiments from the exact model values. The individual pseudodata are obtained by adding to these exact values a random error with a Gaussian distribution [6,37]. We then analyze each pseudoexperiment using the difference method, with the three other theoretical models as comparison models, and determine a value for the coupling constant. The average value for this sample of simulations is obtained to high accuracy. We list the result of this exercise, with all six permutations, in Table IV. The model in quotation marks is the one used to generate the ''experimental'' pseudodata. Here $g^2_{\pi^\pm}$ is the mean value of the coupling constant for the 10 000 pseudoexperiments, while the errors quoted are standard deviations for individual pseudoexperiments.

We now discuss the systematic deviations $\delta g^2_{\pi^\pm}$ of the mean value in the sample from that of the true value in the model (see Table IV). We first note that once $\chi^2/N_{df}$ has reached its minimum plateau close to 1 within a few percent, there are few systematic deviations clearly outside the statistical uncertainty. The principal one occurs in the Bonn B− ''Nijm93'' difference for $n=4$ with $\delta g^2_{\pi^\pm}=-0.50$ ($-3.7\%$). The Bonn B−''NI93'' difference also exhibits a rather large systematic shift $\delta g^2_{\pi^\pm}=-0.43$ for $n=4$. This is to be expected, since the Bonn B − ''NI93'' difference follows mathematically from the NI93 − ''Nijm93'' one for $n=4$, as seen from Table IV. One has

$$\begin{aligned}\delta g^2_{\pi^\pm}&(\text{Bonn B}-\text{``NI93''})\\ &=\delta g^2_{\pi^\pm}(\text{Bonn B}-\text{``Nijm93''})\\ &\quad-\delta g^2_{\pi^\pm}(\text{NI93}-\text{``Nijm93''})\\ &=-0.50+0.07=-0.43.\end{aligned}$$

The Bonn B potential belongs to a previous generation of descriptions of $NN$ observables as compared to the other models. It has a notably worse value for $\chi^2/N_{df}$ with respect to our data than the other models. After adjustment for normalization, the $\chi^2/N_{df}$ is 13.0, as compared to 5.02, 5.64, and 2.6 for Nijm93, NI93, and SM95, respectively. The Bonn B potential gives a larger systematic error than those of a typical realistic modern comparison function.

To summarize, polynomial fits using the difference method for the present experimental data give $n=3$ for the NI93 and Nijm93 models and $n=4$ for the SM95 and Bonn B models. The value for $\chi^2/N_{df}$ is systematically somewhat smaller than 1, which reflects the fact that ten points have

TABLE IV. Values of the coupling constant obtained from polynomial fits with $n$terms to ''pseudodata'' at 96 MeV using the difference method for the range $0<q^2<5.8m_\pi^2$. The comparison models and the model coupling constants are the same as in Table III. $\delta g^2_{\pi^\pm}$ is the systematic shift from the true model value.

| $n$ | $\chi^2/N_{df}$ | $g^2_{\pi^\pm}$ | $\delta g^2_{\pi^\pm}$ | $\chi^2/N_{df}$ | $g^2_{\pi^\pm}$ | $\delta g^2_{\pi^\pm}$ | $\chi^2/N_{df}$ | $g^2_{\pi^\pm}$ | $\delta g^2_{\pi^\pm}$ |
|---|---|---|---|---|---|---|---|---|---|
| | NI93 − ''Nijm93'' | | | SM95 − ''Nijm93'' | | | Bonn B − ''Nijm93'' | | |
| 2 | 1.27 | 13.63 ± 0.04 | −0.05 | 2.56 | 13.49 ± 0.04 | 0.08 | 1.67 | 14.85 ± 0.04 | −1.27 |
| 3 | 1.07 | 13.35 ± 0.10 | 0.23 | 1.62 | 12.86 ± 0.10 | 0.72 | 1.08 | 14.40 ± 0.09 | −0.82 |
| 4 | 1.01 | 13.65 ± 0.20 | −0.07 | 1.01 | 13.82 ± 0.19 | −0.24 | 1.00 | 14.08 ± 0.19 | −0.50 |
| 5 | 1.00 | 13.86 ± 0.42 | −0.28 | 1.00 | 14.06 ± 0.42 | −0.48 | 1.00 | 13.95 ± 0.42 | −0.37 |
| | Bonn B − ''NI93'' | | | Bonn B − ''SM95'' | | | NI93 − ''SM95'' | | |
| 2 | 1.39 | 14.79 ± 0.04 | −1.21 | 2.15 | 15.09 ± 0.04 | −1.34 | 1.56 | 13.90 ± 0.04 | −0.15 |
| 3 | 1.29 | 14.61 ± 0.09 | −1.03 | 2.13 | 15.21 ± 0.09 | −1.46 | 1.29 | 14.22 ± 0.09 | −0.47 |
| 4 | 1.02 | 14.01 ± 0.19 | −0.43 | 1.02 | 14.01 ± 0.19 | −0.26 | 1.00 | 13.58 ± 0.20 | 0.17 |
| 5 | 1.00 | 13.67 ± 0.42 | −0.09 | 1.00 | 13.64 ± 0.42 | 0.11 | 1.00 | 13.55 ± 0.43 | 0.20 |

their errors increased by 25% to account for uncertainties in the carbon subtraction procedure [14], as previously noted. This leads to a decrease of the overall $\chi^2/N_{df}$ by about 0.07, quite apart from the fact that smaller or larger values than 1 normally occurs in a sample. We have chosen to average the values of the four comparison models, and find $g^2_{\pi^\pm}=14.74 \pm 0.14$. The systematic extrapolation uncertainty is determined from the spread of values to be $\pm 0.26(1.8\%)$, while the uncertainty from normalization is 1%, i.e., $\pm 0.15$. Thus the final value for the charged $\pi NN$ coupling constant from the present work is $\sqrt{N}g^2_{\pi^\pm}=14.74\pm 0.14$ (extrapolation and statistical) $\pm 0.26$ (systematic) $\pm 0.15$ (normalization) $=14.74\pm 0.33$. This result is consistent with our previous finding, $\sqrt{N}g^2_{\pi^\pm}=14.52\pm 0.13$ (extrapolation and statistical) $\pm 0.15$ (systematic) $\pm 0.17$ (normalization) $=14.52\pm 0.26$, extracted at 162 MeV [1,2].

## VI. SUMMARY AND CONCLUSIONS

The *np* differential cross section has been measured at 96 MeV using the neutron beam facility at the The Svedberg Laboratory in Uppsala. The data from Rönnqvist *et al.* have been extended to cover the 74°–180° region. The data were normalized using the total *np* cross section, which has been experimentally determined with high precision by Lisowski *et al.* Since our data do not cover the full angular range, the experiment was considered as a measurement of a fraction of the total cross section. This fraction was determined by using the angular shape of a number of energy-dependent PWA's. The data were normalized to the average fraction, obtained from those PWA's, multiplied with the experimental total cross section. We estimate the normalization error to $\pm 1.9\%$.

A general feature is that our data have a steeper slope in the 150°–180° angular region than most of the existing data in the same energy region. As a consequence, the slope is also steeper than several of the current PWA's and *NN* potential models. A similar situation is also present at higher energies, where large data sets disagree significantly in shape.

The *np* scattering cross section at 180° is used as a primary standard for normalization of most other neutron-induced cross sections. Uncertainties of the order of 10% in this cross section are therefore unacceptable. Remeasuring the absolute *np* scattering cross sections with high precision and at several energies should be of high priority.

As a by-product of the present investigation we obtain an extrapolated value $g^2_{\pi^\pm}=14.74\pm 0.33 (f^2_{\pi^\pm}=0.0814 \pm 0.0018)$ for the charged $\pi NN$ coupling constant using the difference method. This is consistent with the value $=14.52\pm 0.26$ found in our previous work at 162 MeV [1,2]. Both these values are 3–6 % higher than those indicated by $\pi N$ data and these problems are presently under debate [4,5]. It is noteworthy that the recent model-independent determination of the coupling constant from the Goldberger-Miyazawa-Oehme (GMO) relation gives a noticeably larger value than those derived from the indirect methods [38]. The present value is within about two standard deviations of this independent new value. Our values depend critically on the absolute normalization of the *np* cross sections, presently inferred indirectly using theoretical assumptions about the unmeasured cross section in the forward hemisphere. These missing data are urgently needed, and are expected to become available in the near future [39] (see below). In addition, directly measured absolutely normalized *np* cross sections in the backward hemisphere are expected to appear on the market within a few years [13].

Our future plans include measurements of *np* scattering between 10° and 170° (c.m.) at a few energies in the 50–180-MeV range. To this end, a new experimental setup is under construction [39]. The new detector system has been designed to detect either recoil protons or scattered neutrons. In this manner, it will be possible to cover both the backward angles by detecting the recoil protons and the forward angles by detecting the scattered neutrons. In particular, we plan to extend the data we have at 96 and 162 MeV to cover the full angular range, i.e., also the forward angles $\theta_{\text{c.m.}}=10°-70°$. By including these forward-angle data, we could normalize our angular distributions to the total *np* cross section directly, without any assumptions about the angular shape.

## ACKNOWLEDGMENTS

We thank The Svedberg Laboratory crew for careful operation of the cyclotron. We are also grateful to M. Lacombe for discussions on contributions to the cross sections for the Paris potential, and to W. R. Gibbs for advice on producing pseudodata from models. T.E. acknowledges an interesting discussion with M. Rentmeester and B.L. acknowledges the hospitality of The Svedberg Laboratory. This work was financially supported by the Swedish Natural Science Research Council and by the CNRS French-Swedish Bilateral Cooperation Program.

[1] T.E.O. Ericson, B. Loiseau, J. Nilsson, N. Olsson, J. Blomgren, H. Condé, K. Elmgren, O. Jonsson, L. Nilsson, P.-U. Renberg, A. Ringbom, T. Rönnqvist, G. Tibell, and R. Zorro, Phys. Rev. Lett. **75**, 1046 (1995).

[2] J. Rahm, J. Blomgren, H. Condé, S. Dangtip, K. Elmgren, N. Olsson, T. Rönnqvist, R. Zorro, A. Ringbom, G. Tibell, O. Jonsson, L. Nilsson, P.-U. Renberg, T.E.O. Ericson, and B. Loiseau, Phys. Rev. C **57**, 1077 (1998).

[3] R. Arndt and R. L. Workman, *Nuclear Data Standards for Nuclear Measurements*, edited by H. Condé, NEANDC-311 ''U''/INDC(SEC)-101 (OECD, Paris, 1992), p. 17; A.D. Carlson, S. Chiba, F.-J. Hambsch, N. Olsson, and A.N. Smirnov, *Update to Nuclear Data Standards for Nuclear Measurements*, edited by H. Wienke, INDC(NDS)-368 (IAEA, Vienna, 1997), p. 9. Data as given by SAID (see Ref. [20]).

[4] M. E. Sainio, *Working Group Summary: Pion-Nucleon Coupling Constant*, 8th International Symposium on Meson-Nucleon Physics and the Structure of the Nucleon, Zuoz, Swit-

zerland, 1999, $\pi$N Newsletter **15**, 171 (1999).
[5] *Proceedings of the Workshop on Critical Issues in the Determination of the Pion-Nucleon Coupling Constant*, Uppsala, 1999 [Phys. Scr. **T87**, 1 (2000)].
[6] B. Loiseau and T.E.O. Ericson, Phys. Scr. **T87**, 53 (2000).
[7] T.E.O. Ericson, B. Loiseau, J. Rahm, N. Olsson, J. Blomgren, H. Condé, K. Elmgren, O. Jonsson, L. Nilsson, P.-U. Renberg, A. Ringbom, T. Rönnqvist, G. Tibell, and R. Zorro, Phys. Rev. Lett. **81**, 5254 (1998).
[8] M.C.M. Rentmeester, R.A.M. Klomp, and J.J. de Swart, Phys. Rev. Lett. **81**, 5253 (1998).
[9] J. Blomgren, N. Olsson, and J. Rahm, Phys. Scr. **T87**, 33 (2000).
[10] B.E. Bonner, J.E. Simmons, C.L. Hollas, C.R. Newsom, P.J. Riley, G. Glass, and Mahavir Jain, Phys. Rev. Lett. **41**, 1200 (1978).
[11] W. Hürster, T. Fischer, G. Hammel, K. Kern, M. Kleinschmidt, L. Lehmann, H. Schmitt, L. Schmitt, and D.M. Sheppard, Phys. Lett. **90B**, 367 (1980); J. Franz, E. Rössle, H. Schmitt, and L. Schmitt, Phys. Scr. **T87**, 14 (2000).
[12] T. E. O. Ericson and W. Weise, *Pions and Nuclei* (Clarendon, Oxford, 1988).
[13] T. Peterson, Phys. Scr. **T87**, 22 (2000); T. Peterson, L.C. Bland, J. Blomgren, W.W. Jacobs, T. Kinashi, A. Klyachko, P. Nadel-Turonski, L. Nilsson, N. Olsson, J. Rapaport, T. Rinckel, E.J. Stephenson, S.E. Vigdor, S.W. Wissink, and Y. Zhou, Nucl. Phys. **A663&664**, 1057c (2000).
[14] T. Rönnqvist, H. Condé, N. Olsson, R. Zorro, J. Blomgren, G. Tibell, O. Jonsson, L. Nilsson, P.-U. Renberg, and S.Y. van der Werf, Phys. Rev. C **45**, R496 (1992).
[15] H. Condé, S. Hultqvist, N. Olsson, T. Rönnqvist, R. Zorro, J. Blomgren, G. Tibell, A. Håkansson, O. Jonsson, A. Lindholm, L. Nilsson, P.-U. Renberg, A. Brockstedt, P. Ekström, M. Österlund, F.P. Brady, and Z. Szeflinski, Nucl. Instrum. Methods Phys. Res. A **292**, 121 (1990).
[16] B. Höistad, E. Nilsson, J. Thun, S. Dahlgren, S. Isaksson, G.S. Adams, and H. Ikegami, Nucl. Instrum. Methods Phys. Res. A **295**, 172 (1990).
[17] R.C. Byrd and W.C. Sailor, Nucl. Instrum. Methods Phys. Res. A **264**, 494 (1989).
[18] R.F. Carlson, At. Data Nucl. Data Tables **63**, 93 (1996).
[19] V.G.J. Stoks, R.A.M. Klomp, M.C.M. Rentmeester, and J.J. de Swart, Phys. Rev. C **48**, 792 (1993). Data as given by SAID (see Ref. [20]).
[20] R.A. Arndt, I.I. Strakovsky, and R.L. Workman, Phys. Rev. C **52**, 2246 (1995); **62**, 034005 (2000). Data as given by Scattering Analysis Interactive Dial-Up (SAID), Virginia Polytechnic Institute, Blackburg, VA (R.A. Arndt, private communication).
[21] P.W. Lisowski, R.E. Shamu, G.F. Auchampaugh, N.S.P. King, M.S. Moore, G.L. Morgan, and T.S. Singleton, Phys. Rev. Lett. **49**, 255 (1982).
[22] D.F. Measday and J.N. Palmieri, Nucl. Phys. **85**, 142 (1966).
[23] V. Grundies, J. Franz, E. Rössle, and H. Schmitt, Phys. Lett. **158B**, 15 (1985).
[24] R.A. Arndt, I.I. Strakovsky, and R.L. Workman, Phys. Rev. C **50**, 2731 (1994).
[25] M. Lacombe, B. Loiseau, J.M. Richard, R. Vinh Mau, J. Côté, P. Pirès, and R. de Tourreil, Phys. Rev. C **21**, 861 (1980).
[26] R. Machleidt, Adv. Nucl. Phys. **19**, 189 (1989); (private communication).
[27] V.G.J. Stoks, R.A.M. Klomp, C.P.F. Terheggen, and J.J. de Swart, Phys. Rev. C **49**, 2950 (1994). Data as given by SAID (see Ref. [20]).
[28] R.H. Stahl and N.F. Ramsey, Phys. Rev. **96**, 1310 (1954).
[29] C.Y. Chih and W.M. Powell, Phys. Rev. **106**, 539 (1957).
[30] J.P. Scanlon, G.H. Stafford, J.J. Thresher, P.H. Bowen, and A. Langsford, Nucl. Phys. **41**, 401 (1963).
[31] A.J. Bersbach, R.E. Mischke, and T.J. Devlin, Phys. Rev. D **13**, 535 (1976).
[32] M. Hammans, C. Brogli-Gysin, S. Burzynski, J. Campbell, P. Haffter, R. Henneck, W. Lorenzon, M.A. Pickar, I. Sick, J.A. Konter, S. Mango, and B. van den Brandt, Phys. Rev. Lett. **66**, 2293 (1991).
[33] R. Henneck, Phys. Rev. C **47**, 1859 (1993).
[34] G.F. Chew, Phys. Rev. **112**, 1380 (1958).
[35] P. Cziffra and M.J. Moravcsik, Phys. Rev. **116**, 226 (1959).
[36] T.E.O. Ericson and B. Loiseau, Phys. Lett. B **393**, 167 (1996).
[37] See, e.g., William R. Gibbs, *Computation in Modern Physics* (World Scientific, Singapore, 1994), p. 35.
[38] T. E. O. Ericson, B. Loiseau, and A. W. Thomas, ''Determination of the pion-nucleon coupling constant and scattering lengths,'' hep-ph/0009312, Phys. Rev. C (submitted).
[39] J. Blomgren, N. Olsson, and the Uppsala Neutron Collaboration, TSL exp. FA104.